Hindawi
Journal of Advanced Transportation
Volume 2022, Article ID 9866794, 14 pages
https://doi.org/10.1155/2022/9866794

Research Article

Disturbance Observer-Smith Predictor Compensation-Based Platoon Control with Estimation Deviation

Jiawei Wang,[1] **Guanpu Wu**,[1] **Bohua Sun**,[1] **Fangwu Ma**,[1] **Bilin Aksun-Guvenc**,[2] **and Levent Guvenc**[2]

[1]*The State Key Laboratory of Automotive Simulation and Control, Jilin University, Changchun 130025, China*
[2]*The Automated Driving Lab, Ohio State University, Columbus, OH 43210, USA*

Correspondence should be addressed to Bohua Sun; bohuasun@jlu.edu.cn

Received 28 May 2022; Revised 23 July 2022; Accepted 5 August 2022; Published 25 August 2022

Academic Editor: Ruimin Ke

In the research of cooperative adaptive cruise control, the coupling relationship between the communication delay, the following time headway, and the string stability leads to a stringent limit on the minimum allowable following time headway. To deal with this limitation, this paper proposes the Disturbance Observer-Smith Predictor Compensation (DOB-SPC)-based Master-Slave architecture. The SPC is adopted to move the communication delays and actuator delays outside the feedback loop in the Master-Slave architecture. It theoretically realizes decoupling when parameters are estimated accurately and achieves zero-headway-string-stability for arbitrary values of communication delay. Subsequently, the robust performance of SPC with estimation deviation of vehicle model dynamic lag, actuator delay, and communication delay in practical application is discussed through the changing trend of the minimum string-stable time headway. To alleviate this problem, the DOB is designed to compensate for the interference caused by the perturbation of vehicle dynamic parameters and improve the estimation accuracy. The simulation results of a four-vehicular platoon show that the string stability and following accuracy are fully guaranteed by applying the proposed strategy, even with smaller headway in the presence of estimation deviation.

1. Introduction

The limited traffic capacity and the increasing road usage demand lead to traffic congestion and the waste of human resources. In response to this phenomenon, Intelligent Transportation Systems (ITS) have emerged for managing transportation networks more accurately and more efficiently. Furthermore, the development of wireless communication, i.e., Cellular Network- Vehicle to Everything (C-V2X) and Dedicated Short Range Communications (DSRC), makes it possible for the ITS system to obtain more information about its surroundings and achieve real-time traffic control in several scenarios and applications, e.g., variable speed advisor [1], ramp metering [2], unsignalized intersection control [3], etc. Platoon control is one of the most promising methods of the intelligent transportation system, which assembles cooperative driving vehicles with a small intervehicular distance to increase traffic efficiency [4, 5]. The longitudinal control of the platoon system, named cooperative adaptive cruise control (CACC), is used to guarantee comfort and safety and has, thus, attracted a large number of researchers over the past few decades [6–9]. CACC technology inherits from adaptive cruise control (ACC) and uses intervehicular communication to receive the information of the surrounding vehicles for longitudinal control decision-making. To some extent, CACC is an intersecting system of integrated communications, vehicle control, and transportation [10, 11]. Several studies focus on platoon communication and design the optimized communication topology to improve the individual vehicle following performance [12, 13]. Researchers in the field of transportation focus on the beneficial effects of CACC on improving traffic efficiency, also including the mixed traffic system [14, 15]. From the perspective of vehicle control, various methods have been proposed to ensure the following accuracy, safety, and comfort under the presence of dynamic uncertainty [16–18].

The biggest difference between ACC and CACC is that CACC technology makes it possible to group a larger

number of vehicles within a small intervehicular distance. To achieve this purpose, more requirements are put forward in the design process of CACC. The most important requirement, string stability, is defined as the attenuation of fluctuation of the leading vehicle's chosen motion variable along the platoon. A string-unstable platoon leads to traffic jams and also makes driving uncomfortable and unsafe. A suitable control architecture like proportional-integral-differential [19], model predictive control [20–22], sliding mode control [23, 24], or optimization control [25–27] and its controller gain tuning must be used to ensure string stability. Following distance strategy is also a way of improving intervehicular following performance. Although constant distance can improve traffic efficiency, it requires a unique communication topological structure to guarantee string stability [28]. The constant headway strategy is the most widely used strategy, and it is quite convenient to reconcile the string stability and traffic efficiency by changing the time headway value [27]. The performance of the designed control architecture can be evaluated by the minimum string-stable time headway and the advantage of CACC in improving traffic efficiency can also be made full use of by applying the minimum string-stable time headway [29, 30].

It should be noted that the advantage of CACC is achieved by the application of intervehicular communication. However, the communication delay is unavoidable and poses a threat to the vehicle following performance [19, 25]. To deal with this challenge, several research studies have adopted the Internet of vehicles–radar (or camera) framework, in which acceleration is transferred by wireless communication and the following distance and velocity difference are detected by radar (or camera), named the traditional architecture [31–34]. Hence, the effect of communication delay only exists in the feedforward loop, and the number of wireless communication packages is greatly reduced. Based on this architecture, the string stability and individual vehicle following accuracy can be guaranteed under the defined communication delay by selecting suitable controller gains. However, as shown in [33], there always exists a maximum allowable communication delay, a value for the designed controller, above which it would be impossible to guarantee the vehicle's following performance. Other papers also reach the same conclusion, and reference [30] further characterizes the corresponding relationship between the minimum allowed time headway and communication time delay. To sum up, the individual vehicle following performance, especially string stability, is strongly coupled with communication time delay and time headway in the traditional architecture. This phenomenon will threaten traffic safety and reduce traffic efficiency when the communication condition is not ideal. Hence, designing a reasonable platoon control architecture that can decouple this relationship or make it weaker is the motivation of this paper.

Smith Predictor Compensation (SPC) is the widely applied method for decoupling the feedback control loop and time delay when the time delay is exactly known [35, 36]. SPC eliminates the time delay of the closed-loop section by moving it outside the feedback loop, thus, guaranteeing that stability will not be lost because of the time delay element. Xing adopted SPC to compensate for the vehicle actuator delay in a CACC system which has led to a smaller value of the minimum string-stable time headway and applied the Master-Slave architecture to create the preconditions for the application of SPC [37]. This research shows that the SPC-based Master-Slave architecture can theoretically guarantee string stability even when time headway is zero. However, the SPC also has its limitation as high estimation accuracy is required to achieve desired control performance. In the application of platoon control, the vehicular dynamic parameters are quite difficult to be estimated accurately, and the presence of various disturbances is also inevitable. Consequently, the performance of SPC in practical application may differ from expectations. This is another motivation of this paper to improve the robustness of SPC in practical application. When affected by model uncertainty, parameter perturbation, and external disturbances, the most effective way to improve the accuracy of SPC prediction is by applying the Disturbance observer (DOB). The core idea of the DOB is to take the difference between the actual output of the controlled object and the output of the nominal model as an equivalent disturbance and compensate it to the control input, thereby eliminating the influence of external disturbances on the control performance of the system. The disturbance observer is generally used as the inner loop of the control system to compensate for the equivalent disturbance, so that the controlled object can present the characteristics of the nominal model as much as possible. Hence, the outer loop controller can be flexibly designed to achieve ideal control performance [38]. Reference [39] proposes a disturbance observer-based hybrid sliding mode impedance control method to achieve robot end constant contact force-tracking control without force/torque sensors. Reference [40] designs disturbance observer-based adaptive control strategy for the flexible air-breathing hypersonic vehicles subject to external disturbances and actuator constraints.

Motivated by these requirements, this paper adopts a similar Master-Slave architecture and SPC to solve the negative influence of communication delay on the vehicle following performance and further adds and designs a DOB to regulate the actual vehicular dynamic model so as to make it behave like its nominal model and reduce estimation deviation of SPC. The main contributions of this paper are summarized below.

(1) The parameter space approach is applied to design the controller gains. This method handles multi-objective controller design very easily, and internal stability, vehicle following accuracy, and string stability are analyzed within this parameter space framework in this research. This approach transfers the performance requirements in the time domain and frequency domain into a feasible region in the chosen parameter space, which forms an intuitive and easily interpreted visual solution region. Then, it is possible to select the controller gains from this

feasible solution region directly and the relationship between following performance and communication time delay is also visualized.

(2) The SPC-based Master-Slave architecture is adopted to implement decoupling of string stability, communication delay, and time headway. Hence, the string stability margin is effectively improved and the limitation of the minimum allowable following headway is significantly reduced, which improves driving comfort and traffic efficiency.

(3) The sensitivity evaluation method of SPC to estimation deviation is proposed by using the variation of minimum string-stable time headway. DOB is designed for the most sensitive factor (the estimation deviation of vehicle model dynamic lag) to improve the prediction accuracy, which realizes the decoupling in the presence of dynamic parameter perturbations.

The remainder of this paper is organized as follows. Section 2 illustrates the platoon dynamic model with Master-Slave architecture and introduces SPC. Section 3 designs the CACC controller by the parameter space approach and compares three different architectures. Section 4 introduces the robustness with estimation deviation and designs the DOB. In Section 5, several numerical simulation results are used to demonstrate the effectiveness of the proposed method. The paper ends with conclusions in section 6.

2. System Modeling

2.1. Master-Slave Architecture. In the traditional architecture, the widely applied CACC controller includes the feedforward section and the feedback section, whose input signals are the communicated value of the acceleration of the preceding vehicle and vehicle following error, respectively. The ego vehicle (vehicle i) receives or detects the input information by wireless communication or on-board radar. The schematic is given in Figure 1. Then, the desired control input u_i are calculated by vehicle i itself. The acceleration of the preceding vehicle provides the intent of that vehicle, as acceleration is the second derivative of position and introduces a positive phase to the system as compared to position and velocity. Using it as feedforward information for the host vehicle introduces phase advance as compared to the mere use of position/velocity information of the preceding vehicle, which improves the stability and bandwidth of the vehicle following system. The communication delay that is present in the feedforward of this acceleration signal limits this improvement.

In order to reduce the degrading effect of communication delay, the Master-Slave architecture in the bottom plot of Figure 1 is used as a first step, which is opposed to the traditional preceding vehicle acceleration feedforward in the top plot of the same figure. The key difference between these two architectures in Figure 1 is that the control input u_i is calculated by different vehicles. In the Master-Slave architecture, the vehicle $i-1$ detects the distance with the follower and calculates the desired control input u_i for vehicle i. Then,

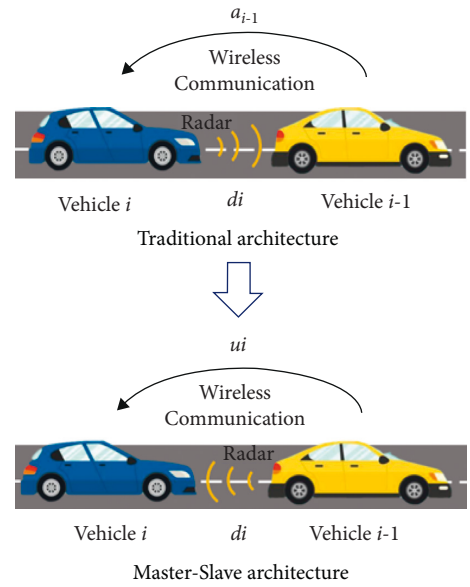

Figure 1: The schematic of traditional architecture and master-slave architecture.

u_i is transferred to vehicle i by wireless communication. In other words, the control input of the ego vehicle is calculated by its preceding vehicle.

To calculate the following error for the feedback section, the constant time headway strategy is utilized in this paper. Then, the desired following distance is expressed as follows:

$$d_{des}(t) = r + hv_i, \tag{1}$$

in which, r is the standstill distance, h is the vehicle following time headway, and v_i is the velocity of the ego vehicle.

Using the actual intervehicular following distance d_i detected by on-board radar, the following error between vehicles i and $i-1$ becomes as follows:

$$e_i(t) = d_i(t) - d_{des}(t). \tag{2}$$

Proportional-Differential (PD) control strategy is applied in the feedback section and the desired control input u_i is calculated as follows:

$$u_{i,tr}(t) = k_p e_i(t) + k_v \dot{e}_i(t) + k_a a_{i-1}(t-\sigma), \tag{3}$$

for the traditional architecture and hence denoted $u_{i,tr}$. k_a in (3) is the preceding vehicle acceleration feedforward gain and the acceleration a_{i-1} of the preceding vehicle is delayed by the intervehicular communication time delay σ. For the Master-Slave architecture, the desired control input u_i is denoted by $u_{i,ms}$ and is given by the following:

$$u_{i,ms}(t) = k_p e_i(t-\sigma) + k_v \dot{e}_i(t-\sigma) + k_a a_{i-1}(t-\sigma), \tag{4}$$

where all the signals are delayed by the intervehicular communication time delay σ as they are calculated by the preceding vehicle $i-1$ and shared by intervehicular communication with the ego vehicle i. Since the time stamp value is also sent along with the communicated control signal in (4), its comparison with the current time in the ego vehicle

will make it possible to determine the exact value of the intervehicular communication delay σ at that time instant. It should be noted that the information sharing between the preceding and ego vehicles is a very basic implementation of collective awareness in a connected vehicle environment. Note that communicated position, velocity, and acceleration information was used successfully in a CACC implementation and highway testing in [41].

Figure 2 shows the control block diagrams of these two architectures, where $F = 1/s^2$ is the double integrator converting acceleration to position, $H = hs + 1$ is the spacing policy, $D = e^{-\sigma s}$ is the intervehicular communication delay, $G_B = k_p + k_v s$ is the feedback PD controller, and $G_F = k_a$ is the acceleration feedforward gain.

As for the vehicle dynamic model in Figure 2, a third-order model with a time lag and actuator delay is often adopted for CACC research. This simplified vehicle dynamic model is given by the following:

$$\begin{cases} \dot{p}(t) = v(t), \\ \dot{v}(t) = a(t), \\ \dot{a}(t) = \dfrac{1}{\tau}u(t-\beta) - \dfrac{1}{\tau}a(t), \end{cases} \tag{5}$$

in which, p, v, a denote the position, the velocity, and the acceleration, respectively; τ is the effective time lag; u expresses the desired acceleration, and β is the actuator delay.

Based on (5), the longitudinal vehicle dynamics in the Laplace domain can be described as follows:

$$G_i(s) = \frac{p_i(s)}{u_i(s)} = \frac{1}{s^2(\tau_i s + 1)} e^{-\beta s}. \tag{6}$$

2.2. SPC-Based Master-Slave Architecture. Figure 3 illustrates the common structure of SPC, where the plant P(s) is decomposed into its delay-free part $P_0(s)$ and the time delay $e^{-\theta s}$ for a plant with time delay. The principle of SPC is estimating the plant model and applying a prediction part $\widehat{P}_0(s)(1 - e^{-\theta s})$ in the feedback section to obtain a system without delay in the characteristic equation. Before applying SPC, the closed loop transfer function between input and output is as follows:

$$\mathcal{G}(s) = \frac{C(s)P_0(s)e^{-\theta s}}{1 + C(s)P_0(s)e^{-\theta s}}. \tag{7}$$

If the prediction part $\widehat{P}_0(s)(1 - e^{-\widehat{\theta s}})$ is well estimated, i.e. $\widehat{P}_0(s) = P_0(s)$, $e^{-\widehat{\theta s}} = e^{-\theta s}$, then the closed loop transfer function becomes as follows:

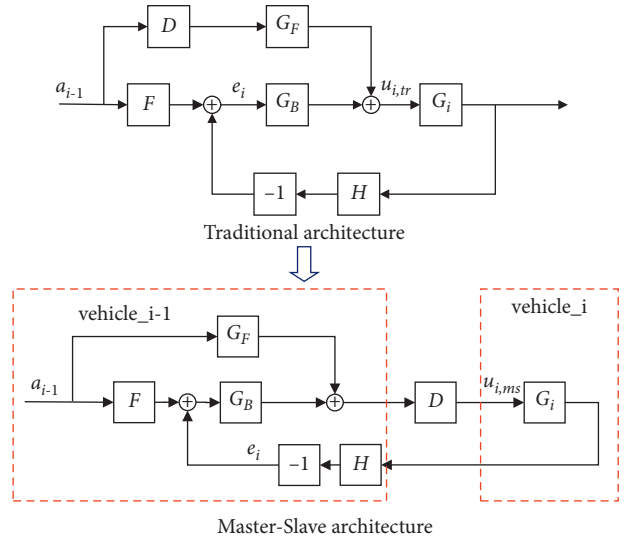

Figure 2: The control block diagrams of these two architectures.

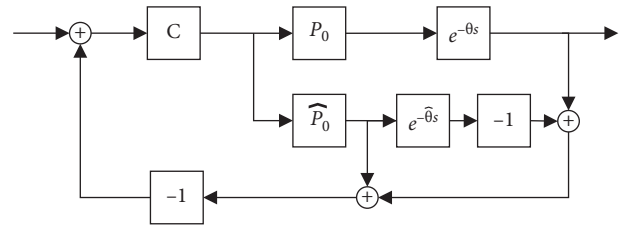

Figure 3: The control block diagrams of SPC.

$$\begin{aligned} \mathcal{G}_{sp}(s) &= \frac{C(s)P_0(s)e^{-\theta s}}{1 + C(s)P_0(s)e^{-\theta s} + C(s)\left(\widehat{P}_0(s) - \widehat{P}_0(s)e^{-\widehat{\theta s}}\right)} \\ &= \frac{C(s)P_0(s)e^{-\theta s}}{1 + C(s)\widehat{P}_0(s)}. \end{aligned} \tag{8}$$

As shown in (8), the time delay does not affect the eigenvalues of the system after perfect SPC compensation.

Applying the SPC into the Master-Slave architecture in Figure 2, the following control block diagram in Figure 4 is obtained.

As shown in Figure 4, $\widehat{G}_i, \widehat{D}$ are adopted to estimate the vehicle dynamic and communication time delay. If the prediction part is well estimated, i.e. $\widehat{G}_i(s) = G_i(s), \widehat{D} = D$, the closed loop transfer function becomes as follows:

$$\Gamma_{sp}(s) = \frac{\left(k_p + k_v s\right) + s^2 k_a}{(\tau s + 1)s^2 + \left(k_p + k_v s\right)(hs + 1)} e^{-(\beta+\sigma)s}, \tag{9}$$

where the overall delay comprising of the inter-vehicular communication delay and the actuator delay have been moved outside of the feedback loop and hence do not affect stability.

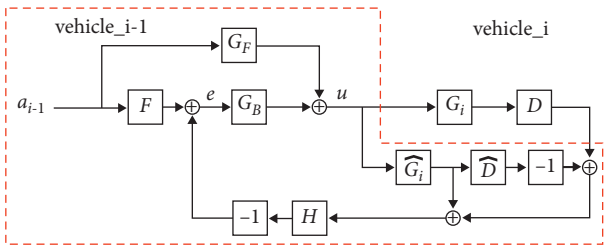

FIGURE 4: The control block diagram of SPC-based master-slave architecture.

3. Parameter Selection and Comparison between Architectures

The control objectives of platoon control mainly include vehicle following accuracy, internal stability, and string stability. The vehicle following accuracy requires the ego vehicle to follow the preceding vehicle with a small following error. Internal stability means the following error converges to zero within a finite time. String stability signifies the characteristic that disturbances are attenuated as we move from one vehicle to the next along the platoon.

3.1. Following Accuracy. For the three architectures of traditional (subscript *tr*), Master-Slave (subscript *ms*), and SPC-based Master-Slave (subscript *spc*) described in Section 2, the transfer functions from the input (a_{i-1}) to the following error (e_i) become the sensitivity transfer functions given by the following:

$$S_{tr}(s) = \frac{(\tau s+1) - k_a(hs+1)e^{-(\sigma+\beta)s}}{(\tau s+1)s^2 + (k_p + k_v s)(hs+1)e^{-\beta s}}, \tag{10}$$

$$S_{ms}(s) = \frac{(\tau s+1) - k_a(hs+1)e^{-(\sigma+\beta)s}}{(\tau s+1)s^2 + (k_p + k_v s)(hs+1)e^{-(\sigma+\beta)s}}, \tag{11}$$

$$S_{spc}(s) = \frac{(\tau s+1) - k_a(hs+1)}{(\tau s+1)s^2 + (k_p + k_v s)(hs+1)}. \tag{12}$$

In order to guarantee vehicle following accuracy, the frequency response magnitudes of the closed loop sensitivity transfer functions in equations (10), (11), and (12) should be close to zero. This guarantees that the vehicle following error will be relatively independent of preceding vehicle acceleration changes. Hence, the acceleration feedforward gains are selected to make the numerators of the sensitivity transfer function in equations (10), (11), and (12) equal to or close to zero by using the following:

$$k_a = \frac{\tau s+1}{hs+1}, \tag{13}$$

which works perfectly only for the SPC compensated Master-Slave architecture in (12).

3.2. Internal Stability. Hurwitz stability is used in internal stability design, which requires the poles to be located on the left-hand side of the imaginary axis in the s-domain. This requirement is enough to make the system convergent, but the convergence characteristics like rate of convergence, overshoot, etc., are not adjustable. In this paper, we define a more restricted $\mathscr{D}$-stability region within the left half plane of the s-domain and require the poles to be located there, as shown in Figure 5 [42].

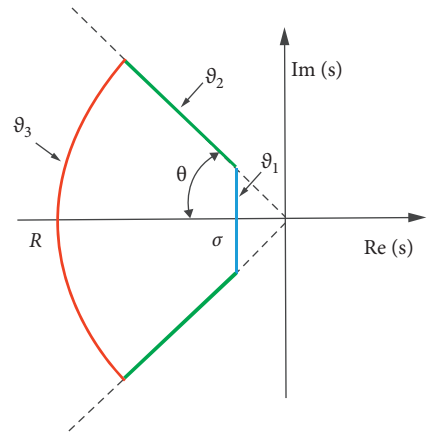

FIGURE 5: $\mathscr{D}$-region in the s-space.

In Figure 5, ϑ_1 reflects the convergence speed, ϑ_2 affects the damping and ϑ_3 limits the bandwidth. Then, the parameter space approach is applied to transfer the $\mathscr{D}$-region from the s-domain to the chosen parameter space of controller gains. This parameter space solution and mapping process is described in detail in reference [42, 43].

When the plant parameters are selected as $\tau = 0.5$ s, $h = 0.6s$, $\beta = 50$ ms, $\sigma = 100$ ms, and the parameters of the $\mathscr{D}$-region are selected as $\sigma = -0.1\pi$, $R = 3\pi$, $\theta = 45^\circ$, the resulting controller parameter space of PD gains for the three different architectures treated here are shown in the same plot in Figure 6 for ease of comparison. If the feedback gains are selected from within the $\mathscr{D}$-stable boundaries shown in Figure 6, the poles of the closed-loop feedback control system would be located inside the $\mathscr{D}$ shaped pole location region in the s-domain, which means that internal stability is well guaranteed. Visual analysis of Figure 6 shows that the SPC-based Master-Slave architecture results in the biggest $\mathscr{D}$-stable controller gain space, which proves that this architecture has the best performance in terms of ensuring internal stability. This is because actuator delay β and communication delay σ have been removed from the denominator of the transfer function S_{sp}. As a result, β and σ do not affect the layout of poles, which is the advantage of using SPC. On the contrary, the $\mathscr{D}$-region of Master-Slave architecture without SPC decreases compared to that of traditional architecture.

Hence, the feedback gains are selected as given in (14) below for the following analysis and simulations and are located in the $\mathscr{D}$-stable regions of all three architectures.

$$k_p = 0.6, \quad k_v = 1.8. \tag{14}$$

3.3. String Stability. Guaranteeing string stability is the biggest challenge to increasing the length of a vehicular

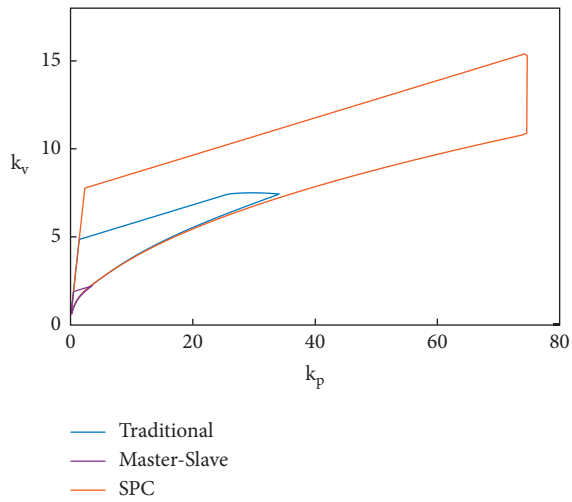

Figure 6: $\mathscr{D}$-region in the parameter space.

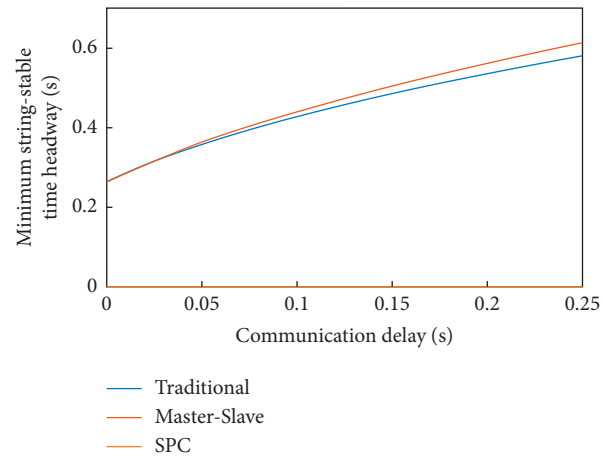

Figure 7: The minimum string-stable time headway of different architectures.

platoon. It means that the fluctuation of the leading vehicle acceleration can be attenuated from one vehicle to the next. The constraint of string stability can be formulated by bounding the magnitude ratio of the transfer function Γ between the preceding vehicle and the ego vehicle pairs and is expressed as follows:

$$\|\Gamma(s)\|_\infty = \left\| \frac{X_i(s)}{X_{i-1}(s)} \right\|_\infty \le 1, \tag{15}$$

for all vehicles in the platoon using the infinity norm. The string stability transfer functions of the three different architectures considered here are given in equations (16), (17), and (18).

$$\Gamma_{tr}(s) = \frac{\left(k_p + k_v s\right)e^{-\beta s} + s^2 k_a e^{-(\sigma+\beta)s}}{(\tau s+1)s^2 + \left(k_p + k_v s\right)(hs+1)e^{-\beta s}}, \tag{16}$$

$$\Gamma_{ms}(s) = \frac{\left(k_p + k_v s + s^2 k_a\right)e^{-(\sigma+\beta)s}}{(\tau s+1)s^2 + \left(k_p + k_v s\right)(hs+1)e^{-(\sigma+\beta)s}}. \tag{17}$$

Especially for $\Gamma_{sp}(s)$, when the feedforward gain is selected as in (13), it further simplifies into the following:

$$\begin{aligned}\Gamma_{sp}(s) &= \frac{\left(k_p + k_v s\right) + s^2(\tau s+1)/(hs+1)}{(\tau s+1)s^2 + \left(k_p + k_v s\right)(hs+1)} e^{-(\sigma+\beta)s} \\ &= \frac{1}{(hs+1)} e^{-(\sigma+\beta)s}.\end{aligned} \tag{18}$$

It is seen that $\Gamma_{sp}(s)$ only includes a lag section $(1/hs+1)$ and a delay section $(e^{-(\sigma+\beta)s})$ after simplification, hence the infinity norm of $\Gamma_{sp}(s)$ is definitely smaller than 1 for frequencies other than d.c. since the first order lag part has a decaying frequency response magnitude starting at one at zero frequency and since the frequency response magnitude of its delay part is always equal to one.

Remark 1. Even when the theoretical time headway h is zero (constant following distance), the string stability can still be ensured for any possible communication time delay when the SPC-based Master-Slave architecture is adopted. This characteristic proves that this architecture decouples the string stability from time headway and communication delay theoretically. When it is applied in platoon control with communication delay, it will still lead to high traffic efficiency.

As for the other two architectures, Figure 7 gives the minimum string-stable time headway when the control gains are selected as (13) and (14). When the communication time delay does not exist, the minimum string-stable time headway of traditional architecture and Master-Slave architecture is 0.264. Then it reaches 0.428 s and 0.44 s, respectively, when the communication time delay is 100 ms.

To sum up, the same feedforward and feedback gains were selected to ensure the following accuracy and internal stability for the three architectures considered in this paper. Then the $\mathscr{D}$-stable region and minimum string-stable time headway were proposed and used to reflect the internal stability and string stability performance measures indirectly. The comparison demonstrated that the SPC architecture has the best performance measures by decoupling the string stability measure from time headway and communication delay.

4. Disturbance Observer-Based Smith Predictor Compensation

The superior performance described in Section 3 can only be achieved when the system parameters are accurately estimated in the SPC, which is more sensitive to estimation deviation. This section analyzes the robust performance of the SPC architecture through the change of the pole distribution and the minimum string-stable time headway and then adds and designs DOB to reduce estimation deviation.

4.1. Robust Performance of SPC with Estimation Deviation. Three parameters are required to be estimated in the SPC architecture. These are the vehicle dynamic lag τ, actuator

delay β, and intervehicular communication time delay σ. Vehicle dynamic lag changes with the driving condition, including actuator characteristics, environment, load, road conditions, etc. Although it is a mature technology to estimate vehicle dynamic lag, a small estimation deviation always exists in the experiment. The actuator delay contains CAN bus transmission delay and internal delay of the actuator. In most cases, the actuator delay is a random and relatively small value, and $\beta \in [20\,\text{ms}, 50\,\text{ms}]$ in this research [33]. The intervehicular communication time delay is also a random value. The standard of the SAE J2735 DSRC Message Set suggests that the transmission frequency of acceleration should be 10 Hz. In most cases, the package can be delivered within one period, and the communication time delay is smaller than 100 ms.

When the estimation deviation exists in the SPC architecture, the string stability transfer function changes to the following:

$$\Gamma_{sp}(s) = \frac{\left(\left(k_p + k_v s\right) + s^2(\tau s + 1)/(hs+1)\right)e^{-(\sigma+\beta)s}}{(\tau s+1)s^2 + \tau s + 1/\tau_m s + 1\left(k_p + k_v s\right)(hs+1) + \ell}, \tag{19}$$

$$\ell = \left(e^{-(\sigma+\beta)s} - \frac{\tau s+1}{\tau_m s+1} e^{-\left(\sigma_m+\beta_m\right)s}\right)\left(k_p + k_v s\right)(hs+1). \tag{20}$$

In which, σ_m, β_m and τ_m are the estimated value of communication delay, actuator delay, and vehicle dynamic lag.

In this paper, the variation ranges of parameters are defined as $\tau \in [0.4\,\text{s}, 0.6\,\text{s}], \beta \in [20\,\text{ms}, 50\,\text{ms}], \sigma_m \in [0\,\text{ms}, 100\,\text{ms}]$. This definition does not mean that the designed SPC is only suitable for the defined parameters and should be viewed only as a numerical illustration example of the application of SPC.

For the random communication delay and actuator delay, the maximum value is adopted to estimate, as σ_m = 100 ms and β_m = 50 ms. To justify this operation, Figure 8 gives the minimum string-stable time headway when applying different estimated values. When the communication delay and the actuator delay are estimated according to the maximum value, the minimum string-stable time headway is controlled within 0.024 s under different delay conditions, which means the impact on the string stability margin is relatively small. If a small value is used for estimation, when the communication delay or the actuator delay is large, the minimum string-stable time headway increases sharply. As shown in Figure 8(d), when the estimated value is 25 ms and 20 ms, if both the communication delay and the actuator delay reach the maximum value, the minimum string-stable time headway increases to 0.384 s, which is much larger than the magnitude of change in Figure 8(a). Therefore, when estimating random communication delay and actuator delay, its maximum value should be used.

As the actual dynamic lag varies from 0.4s to 0.6s, there is a ± 20% estimation deviation. Figure 9 shows the pole distribution with different parameters to demonstrate the internal stability when the estimation deviation exists intuitively. And the communication delay is 100 ms in Figure 9.

It is seen that three of the poles basically remain unchanged, and only one of the poles changes visibly. All poles are located within the $\mathcal{D}$-stable region of the s-domain, which means that internal stability will be guaranteed with the estimation deviation. In addition, it can be seen from (19) that the communication delay and the actuator delay have a similar effect on internal stability, and it can be concluded that the influence of the estimation deviation of communication delay on the characteristic root of the system is also small.

The theoretically minimum string-stable time headway of SPC- is zero when the parameters are estimated accurately. It is obvious that zero headway cannot guarantee string stability when the estimation deviation exists. Figure 10 gives the minimum string-stable time headway under the defined variation ranges when the communication time delay is 0 ms and 100 ms to reflect the string stability of SPC with the estimation deviation.

The following three findings can be summarized according to Figure 10.

(1) The estimation error of the actuator delay hardly influences the string stability. The black line marked in Figure 10 shows the minimum string-stable time headway when the dynamic lag is 0.6s and the actuator delay is varying. The corresponding line changes smoothly under different communication conditions.

(2) The estimation error of dynamic lag has an obvious effect on string stability. The red line marked in Figure 10 shows the minimum string-stable time headway when the actuator delay is 50 ms and dynamic lag is varying. The corresponding line changes sharply under different communication conditions.

(3) The increase in the communication delay amplifies the influence of the estimation deviation on the string stability. When the communication delay does not exist, the estimated deviation range considered in this research increases the minimum string-stable time headway to 0.352 s. And when the communication delay reaches 100 ms, the minimum string-stable time headway reaches 0.375 s. However, its growth rate is much lower than that of the traditional architecture in Figure 7. This phenomenon shows that when accurate prediction cannot be achieved, there is a weak coupling relationship between the communication delay and the string stability. Therefore, the optimization ratio in Table 1 (the reduction ratio of the minimum string-stable time headway) exhibits a phenomenon of increasing with increasing delay.

To sum up, SPC is most sensitive to the estimation error of dynamic lag, which means that the performance would be significantly optimized by improving the estimation

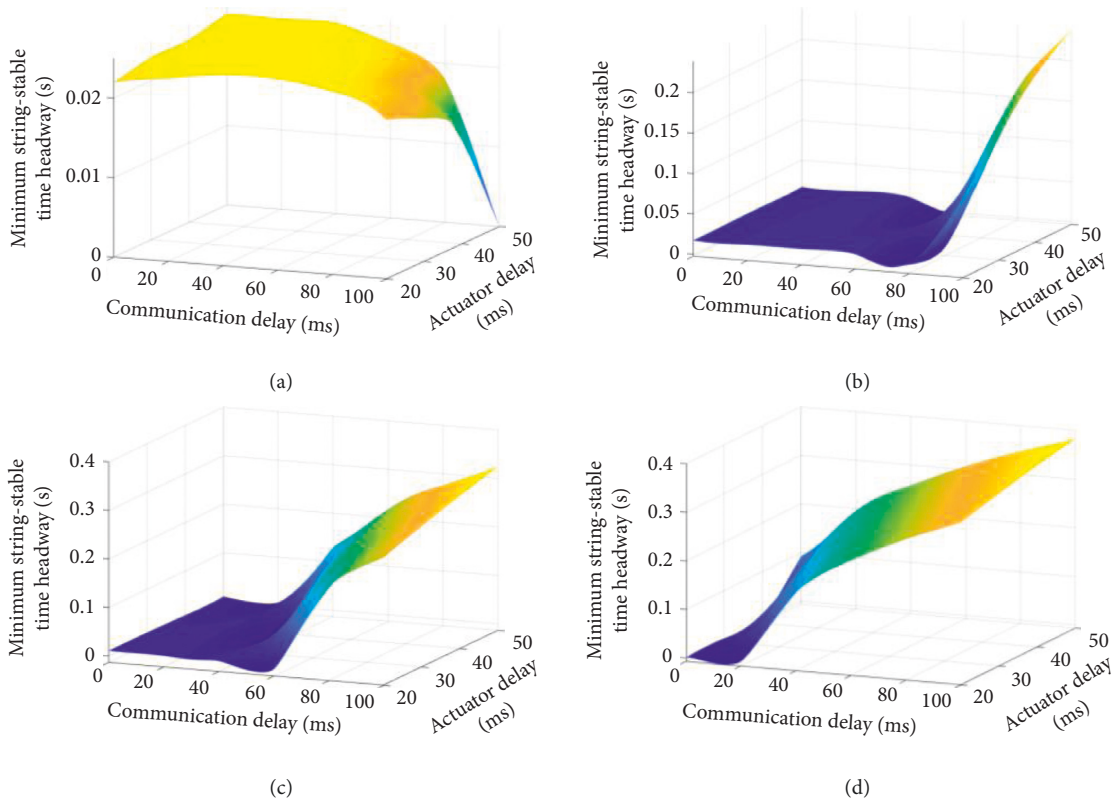

Figure 8: The minimum string-stable time headway with different estimation values of communication delay and actuator delay. (a) σ_m = 100 ms, β_m = 50 ms. (b) σ_m = 75 ms, β_m = 40 ms. (c) σ_m = 50 ms, β_m = 30 ms, (d) σ_m = 25 ms, β_m = 20 ms.

accuracy of the dynamic lag. Table 1 also shows that SPC decreases the minimum string-stable time headway markedly with a high degree of estimation accuracy.

4.2. The Design of DOB-SPC. To overcome the limitation of SPC and improve its robustness, this research adds and designs a disturbance observer loop to make the system behave like its nominal model and avoid the estimation deviation. The architecture of the commonly used DOB is shown in Figure 11. G_n is the nominal model and G is the actual model with multiplicative disturbance as $G = G_n(1 + \Delta m)$. Then, the inverse model of G_n is adopted to estimate the disturbance and the feedback loop with a low-pass filter is designed to force the system to have the desired output as $y = G_n u_n$.

The open loop gain of the disturbance observer compensated plant is as follows:

$$L = \frac{GQ}{G_n(1 - Q)}, \tag{21}$$

and the transfer functions of the model regulation and disturbance rejection are as follows:

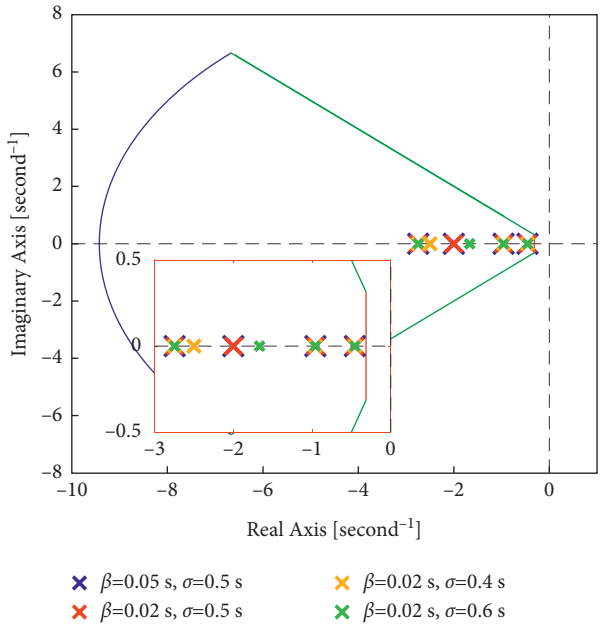

Figure 9: The pole distribution of different architectures.

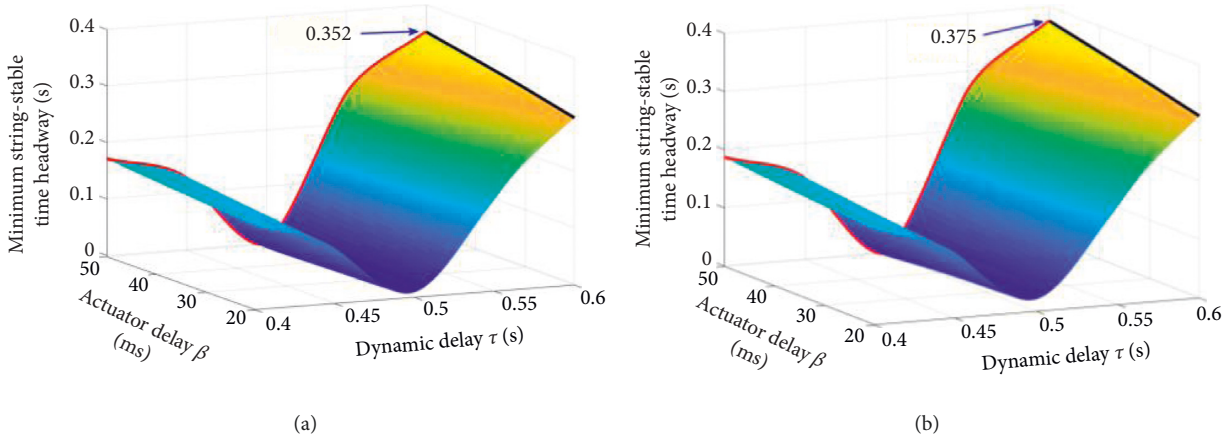

Figure 10: The theoretical minimum string-stable time headway of SPC (a) communication delay is 0 ms; (b) communication delay is 100 ms.

Table 1: The optimization of the minimum string-stable time headway under different estimation accuracy.

Communication delay	0 ms		100 ms	
Estimation deviation	10%	20%	10%	20%
Traditional architecture	0.349s	0.419s	0.482s	0.533s
Master-slave architecture	0.349s	0.419s	0.493s	0.543s
SPC	0.253s	0.352s	0.268s	0.375s
Optimization ratio	27.51	15.99	44.40	29.64

$$\frac{y}{u_n} = \frac{G_n G}{G_n(1-Q)+GQ},$$
$$\frac{y}{d} = \frac{1}{1+L} = \frac{G_n(1-Q)}{G_n(1-Q)+GQ}. \tag{22}$$

As Q is a unity gain low-pass filter, it leads to $y/u_n \longrightarrow G_n, y/d \longrightarrow 0$ at low frequencies, where $Q \longrightarrow 0$. The core of disturbance observer design is to select a suitable low-pass filter. The requirements and the design method of the Q-filter have been introduced in [38], and interested readers should refer to this reference. Then, the sufficient conditions of the Q-filter are summarized as follows:

(1) $|Q| < |1/\Delta m|$, in which $|1/\Delta m| = |G_n/G - G_n|$

(2) Make the filter Q/G_n causal and hence implementable.

Applying DOB-SPC for platoon control, the block diagram that is proposed and used is illustrated in Figure 12.

In Figure 12, the nominal model G_n and the estimation model $\widehat{G}_i$ are the same, as follows:

$$G_n(s) = \widehat{G}_i(s) = \frac{1}{s^2(\tau_n s + 1)}. \tag{23}$$

It should be noted that the actuator delay β is eliminated in the nominal model as its effect was seen to be minimal (discussed in Section 4.1). It is regarded as disturbance and regulated by DOB.

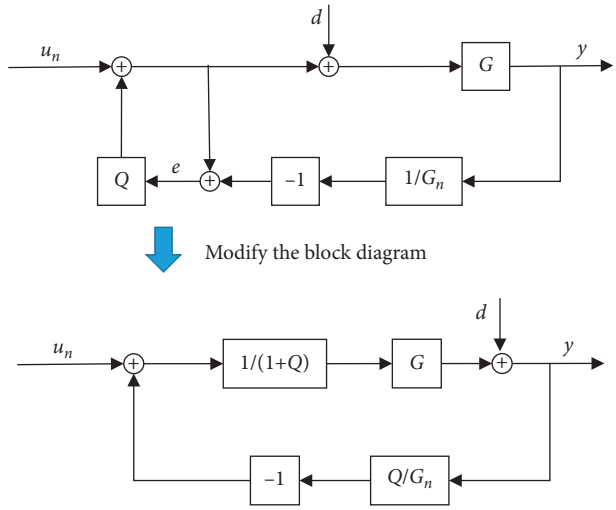

Figure 11: The architecture of the disturbance observer.

The boundary of the multiplicative disturbance is as follows:

$$\frac{1}{\Delta m(j\omega)} = \frac{\tau_{max} j\omega + 1}{\left(\tau_n e^{-\beta_{max} j\omega} - \tau_{max}\right) j\omega + e^{-\beta_{max} j\omega} - 1},$$
$$\frac{1}{\Delta m(j\omega)} = \frac{\tau_{min} j\omega + 1}{\left(\tau_n e^{-\beta_{max} j\omega} - \tau_{min}\right) j\omega + e^{-\beta_{max} j\omega} - 1}, \tag{24}$$

in which $\tau_{max} = 0.6s$, $\tau_{min} = 0.4s$, $\tau_n = 0.5s$, $\beta_{max} = 50$ ms.

The energy of the vehicle longitudinal velocity power spectrum is mainly distributed around 0~1.15 Hz. Therefore, the Q-filter is chosen as a third-order low-pass filter with a relative degree of three given by the following:

$$Q(s) = \frac{1}{0.05^3 s^3 + 3 \times 0.05^2 s^2 + 3 \times 0.05 s + 1}. \tag{25}$$

The third-order relative degree filter makes the other filter Q/G_n causal. The Q-filter selected by equation (25) is shown as the yellow line in Figure 13, which satisfies the requirement that $|Q| < |1/\Delta m|$. The cut-off frequency of the

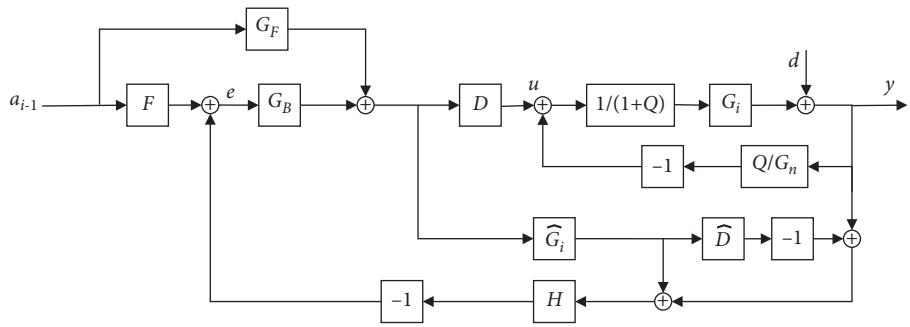

Figure 12: The block diagram of DOB-SPC.

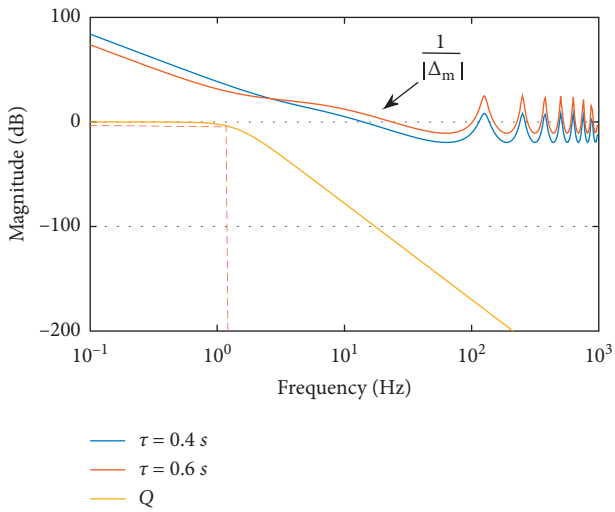

Figure 13: The verification of the Q-filter design requirement.

Table 2: The parameters applied in the simulation.

Parameter	Value
τ	[0.4 s, 0.6 s]
β	[20 ms, 50 ms]
k_p	0.6
k_v	1.8
k_a	$\frac{\tau s+1}{hs+1}$

low-pass filter is about 6.7 Hz, and its amplitude is approximately 1 in the frequency range of 0~1.15 Hz.

5. Numerical Simulation

To further verify the correctness and effectiveness of the CACC controller and DOB-SPC architecture proposed here, several numerical simulation results are presented in this section. This research simulates a four-vehicular platoon by Matlab/Simulink and the HWFET (Highway Fuel Economy Test) standard drive cycle is applied for the lead vehicle speed profile. Two sets of simulations are conducted, one with estimation deviation and one without. The parameters used in the simulations are listed in Table 2.

5.1. Simulation without Estimation Deviation. When the communication delay is 100 ms, the minimum string-stable time headway of the traditional architecture is 0.428 s. In the simulations, the corresponding time headway is selected as 0.4 s, which is a little smaller than the minimum allowable value. Figure 14 shows the time response of the four-vehicular platoon. The fluctuation range of the acceleration profiles of each vehicle in Figure 14(a) is generally similar, but there is still a certain degree of overshoot in some time periods (around 30 s). This phenomenon indicates that a pretty large time headway is required when the communication delay exists and that string stability is strongly coupled with communication delay and following headway.

In contrast to the traditional architecture, which exhibited string stability problems, the SPC decouples the communication delay and string stability when the parameters are well estimated. Figure 15 shows the simulation results of SPC with the same headway ($h = 0.4s$). From the acceleration response, this control strategy makes the acceleration fluctuations attenuate continuously during the transmission to followers, which effectively improves the ride comfort. The acceleration root mean square value of the tail vehicle is attenuated from 0.402 m/s^2 of the lead vehicle to 0.396 m/s^2. The comparison of acceleration root mean square values in two different architectures is given in Figure 16. Otherwise, the following accuracy achieved by SPC is similar to the following accuracy in traditional architecture. In summary, SPC improves the margin of string stability and achieves a smoother following.

5.2. Simulation with Estimation Deviation. In the simulation, the communication delay is estimated as 100 ms, while the actual value is random and smaller than 100 ms. The actuator delay is estimated as 50 ms, while the actual value is random as [20ms, 50ms], and vehicle dynamic lag contains ± 20% estimation deviation. Specifically, the estimation value is 0.5s, but the actual value of vehicles varies within [0.4 s, 0.6 s] in the whole process of simulation. To make the results comparable and verify the effectiveness of the disturbance observer, the headway is also selected as $h = 0.4s$, which is slightly larger than the minimum string-stable time headway (0.375 s) shown in Table 1.

Figures 17 and 18 give the simulation results of SPC and DOB-SPC, and Figure 19 gives the comparison of acceleration root mean square values in two sets of simulation

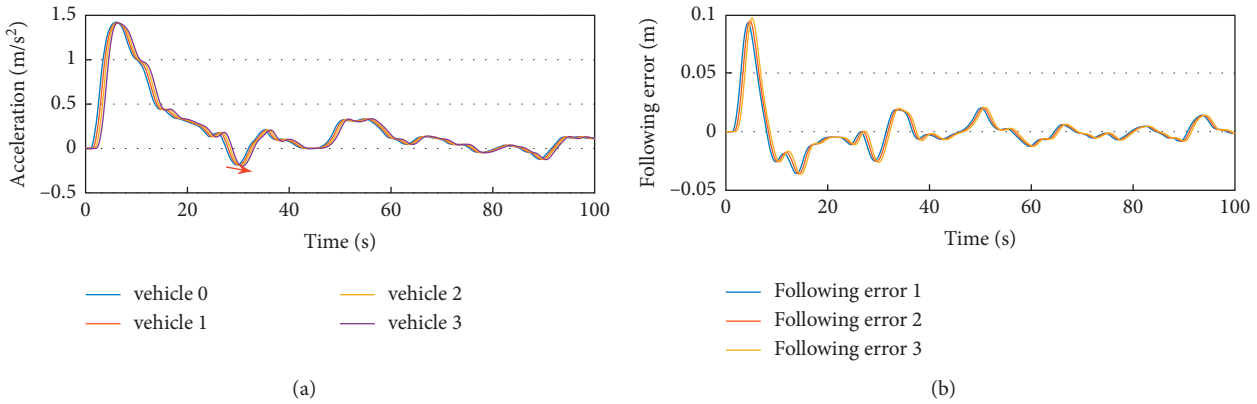

Figure 14: The simulation results of traditional architecture.

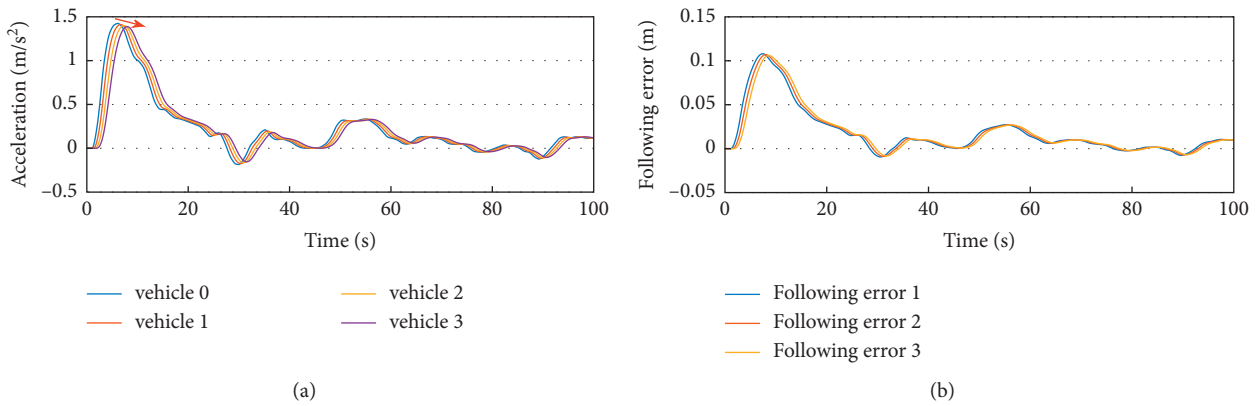

Figure 15: The simulation results of SPC under HWFET.

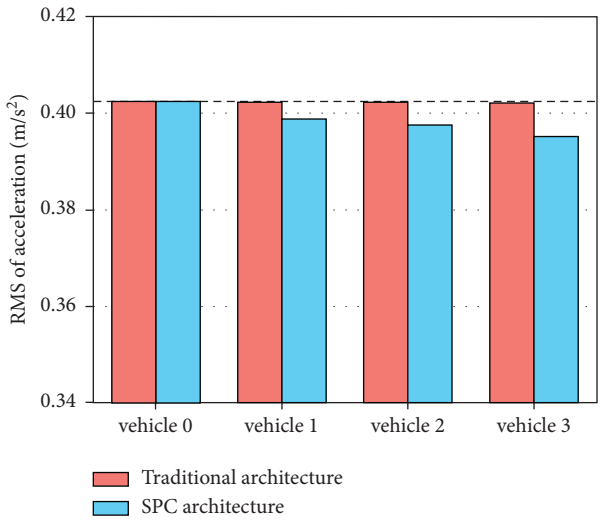

Figure 16: The comparison of acceleration root mean square values in two different architectures.

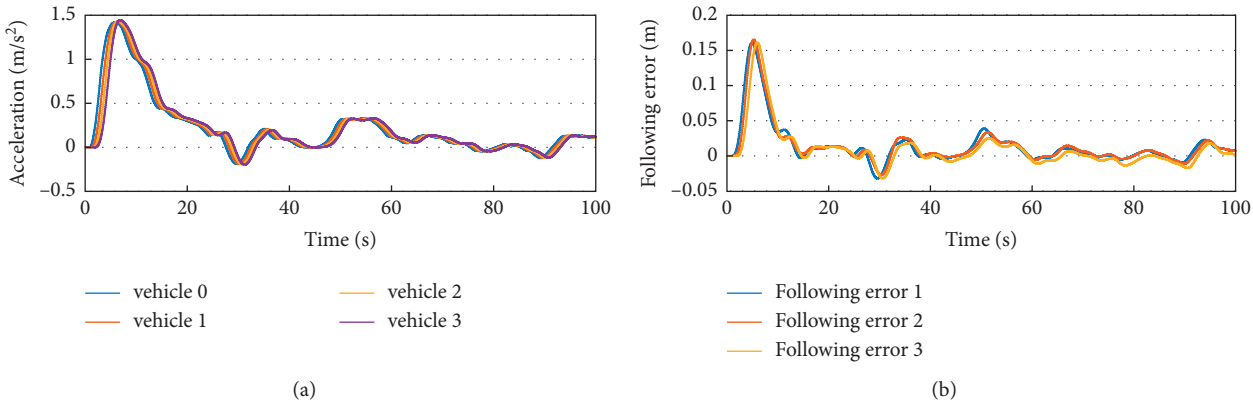

Figure 17: The simulation results of SPC with estimation deviation.

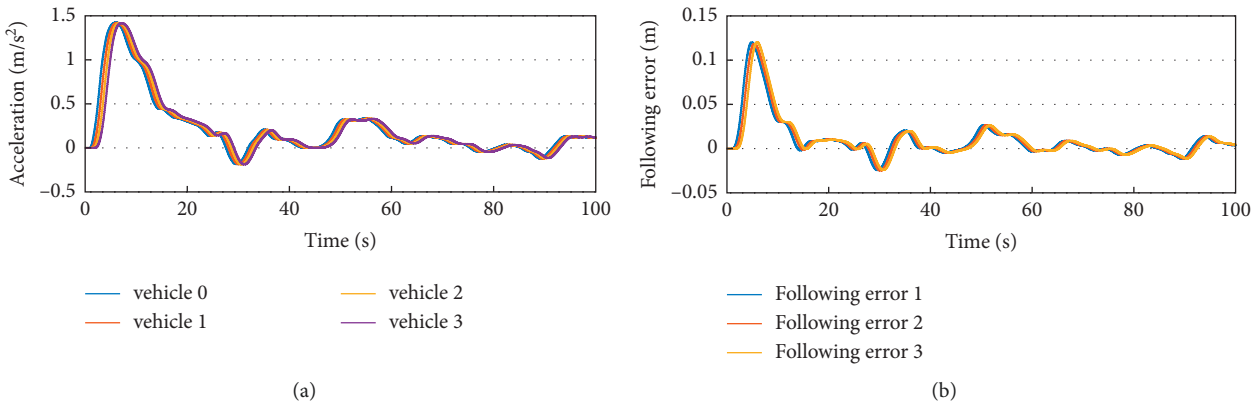

Figure 18: The simulation results of DOB-SPC with estimation deviation.

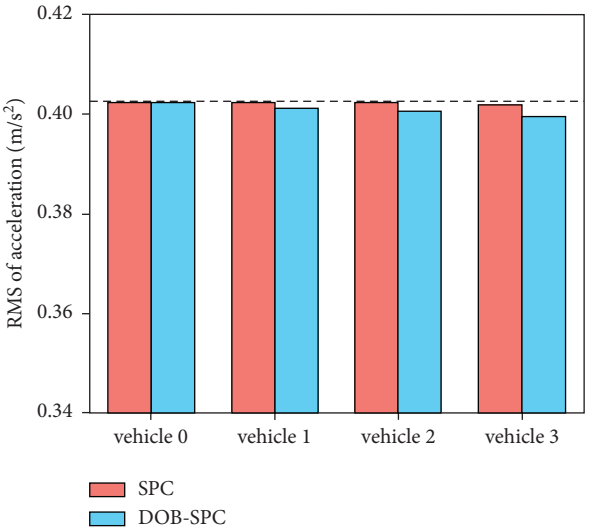

Figure 19: The comparison of acceleration root mean square values in two sets of simulation results.

results. From Figure 19, both sets of results can make the acceleration RMS value show a decaying trend, but when the disturbance observer is not used, the decaying amplitude is not obvious, mainly because the following headway is only slightly larger than the minimum string-stable time headway. But Figure 17(a) shows that during the first 10s of acceleration, the acceleration of the following vehicle has a small overshoot, which is contrary to the definition of chord stability. In other cases, the following performance is ideal, and there is no increase in acceleration fluctuations. Therefore, when there is a 20% estimation deviation, the SPC cannot guarantee the string stability of the vehicular platoon under the condition of large acceleration. After adopting the disturbance observer, the attenuation range of the acceleration RMS value has increased, and the acceleration RMS value of vehicle 3 is attenuated from 4.023 m/s^2 of the leading vehicle to 3.992 m/s^2, which means the string stability margin is increased. Figure 18(a) shows that the acceleration profiles of the following vehicles are smoother than the result in Figure 17(a) and without any overshoot during the entire following process. In addition, comparing Figures 17(b) and 18(b), it can be found that the following error is reduced by about 25% after adding the disturbance observer. To sum up, DOB-SPC is not only beneficial to improve the string stability margin and ensure driving comfort but also can improve the following accuracy.

6. Conclusion

In this paper, the DOB-SPC-based Master-Slave architecture was adopted to decouple string stability from communication delay and vehicle following time headway. The

Master-Slave architecture was designed firstly, in which the preceding vehicle detects the distance with its follower, then calculates and delivers the desired acceleration for its follower. The SPC was proposed to offset the communication delay and actuator delay in the Master-Slave architecture. The DOB was designed to reduce the estimation deviation and improve the robustness of SPC in practical application. Then, the performance of the DOB-SPC was evaluated by simulation results of a four-vehicular platoon.

When the parameters are estimated accurately, SPC can realize zero-headway-string-stability in any case of communication delay. Hence, the traffic efficiency can be significantly improved, and the effect of communication delay on string stability is eliminated. Considering the estimation deviation in the practical application, SPC still weakens the coupling between headway and string stability, and a relative minimum string-stable time headway is achieved. It also demonstrates that improving the estimation accuracy of dynamic lag is the most efficient method to reduce minimum string-stable time headway. Motivated by this finding, the designed disturbance observer makes the plant with disturbance behave like its nominal model to avoid estimation deviation. The simulation results show that DOB-SPC guarantees the string stability and following accuracy even when quite small headway is chosen.

In future research work, we will consider the heterogeneous platoons and communication disturbance observer.

Data Availability

The data used to support the findings of this study can be obtained from the corresponding author upon request.

Conflicts of Interest

The authors declare that they have no conflicts of interest.

Acknowledgments

The work of the first four authors was supported by the National Nature Science Foundation of China, under Grant no. 52102457, and the Jilin Provincial Key Laboratory of Future Eco-Mobility, under Grant no. YDZJ202102CXJD017.

References

[1] X.-Y. Lu, P. Varaiya, R. Horowitz, D. Su, and S. E. Shladover, "A New Approach for Combined Freeway Variable Speed Limits and Coordinated Ramp Metering," in *Proceedings of the 13th International IEEE Conference on Intelligent Transportation Systems*, pp. 491–498, Funchal, Portugal, September2010.

[2] W. Cao, M. Mukai, T. Kawabe, H. Nishira, and N. Fujiki, "Cooperative vehicle path generation during merging using model predictive control with real-time optimization," *Control Engineering Practice*, vol. 34, pp. 98–105, 2015.

[3] W. Yao, N. Jia, S. Zhong, and L. Li, "Best response game of traffic on road network of non-signalized intersections," *Physica A: Statistical Mechanics and Its Applications*, vol. 490, pp. 386–401, 2018.

[4] A. Ghasemi and S. Rouhi, "Stability analysis of a predecessor-following platoon of vehicles with two time delays," *Promet - Traffic & Transportation*, vol. 27, no. 1, pp. 35–46, 2015.

[5] Y. Zheng, S. E. Li, K. Li, and L. Y. Wang, "Stability margin improvement of vehicular platoon considering undirected topology and asymmetric control," *IEEE Transactions on Control Systems Technology*, vol. 24, no. 4, pp. 1253–1265, 2016.

[6] Y. Zheng, S. E. Li, K. Li, and W. Ren, "Platooning of connected vehicles with undirected topologies: robustness analysis and distributed H-infinity controller synthesis," *IEEE Transactions on Intelligent Transportation Systems*, vol. 19, no. 5, pp. 1353–1364, 2018.

[7] W. Yue and L. Wang, "Robust exponential H∞ control for autonomous platoon against actuator saturation and time-varying delay," *International Journal of Control, Automation and Systems*, vol. 15, no. 6, pp. 2579–2589, 2017.

[8] V. Milanés and S. E. Shladover, "Modeling cooperative and autonomous adaptive cruise control dynamic responses using experimental data," *Transportation Research Part C: Emerging Technologies*, vol. 48, pp. 285–300, 2014.

[9] Y. Liu, C. Pan, H. Gao, and G. Guo, "Cooperative spacing control for interconnected vehicle systems with input delays," *IEEE Transactions on Vehicular Technology*, vol. 66, no. 12, pp. 10692–10704, 2017.

[10] Z. Wang, Y. Bian, S. E. Shladover, G. Wu, S. E. Li, and M. J. Barth, "A survey on cooperative longitudinal motion control of multiple connected and automated vehicles," *IEEE Intelligent Transportation Systems Magazine*, vol. 12, no. 1, pp. 4–24, 2020.

[11] Y. Zheng, S. Eben Li, J. Wang, D. Cao, and K. Li, "Stability and scalability of homogeneous vehicular platoon: study on the influence of information flow topologies," *IEEE Transactions on Intelligent Transportation Systems*, vol. 17, no. 1, pp. 14–26, 2016.

[12] S. E. Li, X. Qin, Y. Zheng, J. Wang, K. Li, and H. Zhang, "Distributed platoon control under topologies with complex eigenvalues: stability analysis and controller synthesis," *IEEE Transactions on Control Systems Technology*, vol. 27, no. 1, pp. 206–220, 2019.

[13] S. Feng, Y. Zhang, S. E. Li, Z. Cao, H. X. Liu, and L. Li, "String stability for vehicular platoon control: definitions and analysis methods," *Annual Reviews in Control*, vol. 47, pp. 81–97, 2019.

[14] H. Liu, X. D. Kan, S. E. Shladover, X.-Y. Lu, and R. E. Ferlis, "Modeling impacts of Cooperative Adaptive Cruise Control on mixed traffic flow in multi-lane freeway facilities," *Transportation Research Part C: Emerging Technologies*, vol. 95, pp. 261–279, 2018.

[15] H. Liu, X. D. Kan, S. E. Shladover, X.-Y. Lu, and R. E. Ferlis, "Impact of cooperative adaptive cruise control on multilane freeway merge capacity," *Journal of Intelligent Transportation Systems*, vol. 22, no. 3, pp. 263–275, 2018.

[16] H. Chehardoli and A. Ghasemi, "Adaptive centralized/decentralized control and identification of 1-D heterogeneous vehicular platoons based on constant time headway policy," *IEEE Transactions on Intelligent Transportation Systems*, vol. 19, no. 10, pp. 3376–3386, 2018.

[17] V. S. Dolk, J. Ploeg, and W. P. M. H. Heemels, "Event-Triggered control for string-stable vehicle platooning," *IEEE Transactions on Intelligent Transportation Systems*, vol. 18, no. 12, pp. 3486–3500, 2017.

[18] J. I. Ge and G. Orosz, "Dynamics of connected vehicle systems with delayed acceleration feedback," *Transportation Research Part C: Emerging Technologies*, vol. 46, pp. 46–64, 2014.

[19] W. B. Qin, M. M. Gomez, and G. Orosz, "Stability and frequency response under stochastic communication delays with applications to connected cruise control design," *IEEE Transactions on Intelligent Transportation Systems*, vol. 18, no. 2, pp. 388–403, 2017.

[20] H. Kazemi, H. N. Mahjoub, A. Tahmasbi-Sarvestani, and Y. P. Fallah, "A learning-based stochastic MPC design for cooperative adaptive cruise control to handle interfering vehicles," *IEEE Transactions on Intelligent Vehicles*, vol. 3, no. 3, pp. 266–275, 2018.

[21] E. van Nunen, J. Reinders, E. Semsar-Kazerooni, and N. van de Wouw, "String stable model predictive cooperative adaptive cruise control for heterogeneous platoons," *IEEE Transactions on Intelligent Vehicles*, vol. 4, no. 2, pp. 186–196, 2019.

[22] G. J. L. Naus, J. Ploeg, M. J. G. Van de Molengraft, W. P. M. H. Heemels, and M. Steinbuch, "Design and implementation of parameterized adaptive cruise control: an explicit model predictive control approach," *Control Engineering Practice*, vol. 18, no. 8, pp. 882–892, 2010.

[23] Y. Wu, S. E. Li, J. Cortes, and K. Poolla, "Distributed sliding mode control for nonlinear heterogeneous platoon systems with positive definite topologies," *IEEE Transactions on Control Systems Technology*, vol. 28, no. 4, pp. 1272–1283, 2020.

[24] M. Yan, J. Song, L. Zuo, and P. Yang, "Neural adaptive sliding-mode control of a vehicle platoon using output feedback," *Energies*, vol. 10, no. 11, pp. 1906–1917, 2017.

[25] W. Gao, Z.-P. Jiang, and K. Ozbay, "Data-driven adaptive optimal control of connected vehicles," *IEEE Transactions on Intelligent Transportation Systems*, vol. 18, no. 5, pp. 1122–1133, 2017.

[26] J. I. Ge and G. Orosz, "Optimal control of connected vehicle systems with communication delay and driver reaction time," *IEEE Transactions on Intelligent Transportation Systems*, vol. 18, no. 8, pp. 2056–2070, 2017.

[27] Y. Zhu, D. Zhao, and Z. Zhong, "Adaptive optimal control of heterogeneous CACC system with uncertain dynamics," *IEEE Transactions on Control Systems Technology*, vol. 27, no. 4, pp. 1772–1779, 2019.

[28] Y. Zheng, S. E. Li, K. Li, F. Borrelli, and J. K. Hedrick, "Distributed model predictive control for heterogeneous vehicle platoons under unidirectional topologies," *IEEE Transactions on Control Systems Technology*, vol. 25, no. 3, pp. 899–910, 2017.

[29] G. J. L. Naus, R. P. A. Vugts, J. Ploeg, M. J. G. van de Molengraft, and M. Steinbuch, "String-stable CACC design and experimental validation: a frequency-domain approach," *IEEE Transactions on Vehicular Technology*, vol. 59, no. 9, pp. 4268–4279, 2010.

[30] J. Ploeg, E. Semsar-Kazerooni, G. Lijster, N. van de Wouw, and H. Nijmeijer, "Graceful degradation of cooperative adaptive cruise control," *IEEE Transactions on Intelligent Transportation Systems*, vol. 16, no. 1, pp. 488–497, 2015.

[31] H. Xing, J. Ploeg, and H. Nijmeijer, "Padé approximation of delays in cooperative ACC based on string stability requirements," *IEEE Transactions on Intelligent Vehicles*, vol. 1, no. 3, pp. 277–286, 2016.

[32] M. T. Emirler, L. Güvenç, and B. A. Güvenç, "Design and evaluation of robust cooperative adaptive cruise control systems in parameter space," *International Journal of Automotive Technology*, vol. 19, no. 2, pp. 359–367, 2018.

[33] F. Ma, J. Wang, S. Zhu et al., "Distributed control of cooperative vehicular platoon with nonideal communication condition," *IEEE Transactions on Vehicular Technology*, vol. 69, no. 8, pp. 8207–8220, 2020.

[34] F. Ma, J. Wang, Y. Yu et al., "Parameter-space-based robust control of event-triggered heterogene-ous platoon," *IET Intelligent Transport Systems*, vol. 15, no. 1, pp. 61–73, 2021.

[35] C. Yin, J. Gao, and Q. Sun, "Enhanced PID controllers design based on modified Smith predictor control for unstable process with time delay," *Mathematical Problems in Engineering*, vol. 2014, pp. 1–7, 2014.

[36] M. Bettayeb, R. Mansouri, U. Al-Saggaf, and I. M. Mehedi, "Smith predictor based fractional-order-filter PID controllers design for long time delay systems," *Asian Journal of Control*, vol. 19, no. 2, pp. 587–598, 2017.

[37] H. Xing, J. Ploeg, and H. Nijmeijer, "Compensation of communication delays in a CooperativeACCSystem," *IEEE Transactions on Vehicular Technology*, vol. 69, no. 2, pp. 1177–1189, 2020.

[38] L. Guvenc, B. Aksun-Guvenc, B. Demirel, and M. T. Emirler, *Control of Mechatronic Systems*, IET, London, UK, 2017.

[39] T. Zhang and X. Liang, "Disturbance Observer-Based Robot End Constant Contact Force-Tracking Control," *Complexity*, 2019.

[40] G. Wang, L. Li, W. Li, H. Zhou, C. Ma, and H. Xia, "Disturbance observer-based adaptive control of hypersonic vehicles with constrained actuators," *International Journal of Aerospace Engineering*, pp. 1–12, 2020.

[41] L. Guvenc, I. M. C. Uygan, K. Kahraman et al., "Cooperative adaptive cruise control implementation of team mekar at the grand cooperative driving challenge," *IEEE Transactions on Intelligent Transportation Systems*, vol. 13, no. 3, pp. 1062–1074, 2012.

[42] S. Zhu, S. Y. Gelbal, B. Aksun-Guvenc, and L. Guvenc, "Parameter-space based robust gain-scheduling design of automated vehicle lateral control," *IEEE Transactions on Vehicular Technology*, vol. 68, no. 10, pp. 9660–9671, 2019.

[43] J. Wang, F. Ma, Y. Yang, J. Nie, B. Aksun-Guvenc, and L. Guvenc, "Adaptive event-triggered platoon control under unreliable communication links," *IEEE Transactions on Intelligent Transportation Systems*, vol. 23, no. 3, pp. 1924–1935, 2022.